



Ethylene diffusion in crystals of zeolitic imidazole Framework-11 embedded in polymers to form mixed-matrix membranes

Evan M. Forman^a, Amineh Baniani^a, Lei Fan^a, Kirk J. Ziegler^a, Erkang Zhou^b, Fengyi Zhang^b, Ryan P. Lively^b, Sergey Vasenkov^{a,*}

^a Department of Chemical Engineering, University of Florida, Gainesville, FL 32611, USA

^b School of Chemical & Biomolecular Engineering, Georgia Institute of Technology, Atlanta, GA, 30332, USA

ARTICLE INFO

Keywords:

Diffusion
PFG NMR
MOF
Mixed-matrix membrane

ABSTRACT

¹³C Pulsed field gradient (PFG) NMR was used to study the self-diffusion of ethylene in loosely packed beds of ZIF-11 crystals and ZIF-11 based mixed matrix membranes (MMMs) at different sorbate loadings and diffusion times. The ZIF-11 based MMMs were formed by embedding ZIF-11 crystals in one of the following three polymers: Torlon, Matrimid, and 6FDA-DAM. PFG NMR data allowed obtaining ethylene diffusivities inside ZIF-11 crystals in the crystal beds and MMMs under the same or similar conditions. It was observed that the intra-ZIF diffusivities in ZIF-11/Torlon MMM are smaller than the corresponding diffusivities in the ZIF-11 bed. The observed diffusivity reduction becomes less significant with increasing ethylene loading. At the same time, within uncertainty, no difference in the intra-ZIF diffusivities between ZIF-11 bed and MMMs were observed for ZIF-11/Matrimid and ZIF-11/6FDA-DAM MMMs. The intra-ZIF diffusivity reduction observed for ZIF-11/Torlon MMM is tentatively attributed to the reduced framework flexibility of ZIF-11 crystals once embedded in the Torlon to form the MMM. The absence of such diffusivity reduction in the other two studied MMMs is tentatively explained by the higher bulk modulus of Torlon compared to Matrimid and 6FDA-DAM.

1. Introduction

Membrane-based gas separations can provide a reduction in energy consumption and cost compared to typical separation processes like distillation [1–6]. One promising technology is mixed matrix membranes (MMMs), which consist of permeable filler particles embedded within a dense polymer matrix [6–10]. More specifically, MMMs have piqued interest due to their simple, economic fabrication methods, and potential for high-performance gas separations. These advanced hybrid membranes are designed to combine the high-performing separation properties of the filler particle with the ease of fabrication and mechanical properties of pure polymeric membranes [4,8–13]. With the selection of an appropriate filler phase, MMMs have been shown in both experimental and simulation work to improve separation performance relative to the neat polymer phase for challenging gas mixtures, such as carbon dioxide/methane [4–6,10,11,14,15] and olefin/paraffin mixtures [9,16,17]. Recently, zeolitic imidazole frameworks (ZIFs) have been incorporated into polymer matrices as molecular sieves [3,5,8–14,17–19]. The ZIF family has great chemical and thermal stability, while their high surface area, tunable pore aperture size, and

functionality make them intrinsically more compatible with polymers compared to other types of filler particles [5,8,9,11,12,14].

Although most studies have focused on ZIF-8 as the filler material, ZIF-11 [13,14] and ZIF-90 [3,11] have also been considered in MMMs. In particular, ZIF-11 consists of benzimidazole ligands and Zn²⁺ nodes arranged in a RHO topology, whereas ZIF-8 consists of methylimidazole ligands and Zn²⁺ nodes arranged in a SOD topology. Structures of these ZIFs are well described and shown in Refs. [20,21]. ZIFs are known for their framework flexibility, which allows molecules larger than the ZIF pore aperture to diffuse through. Some simulation studies have explored the transport properties of ZIF-8 accounting for this flexibility [22,23]. Our recent ¹³C pulsed field gradient (PFG) NMR studies of sorbate diffusion in a ZIF-8/6FDA-DAM (where 6FDA-DAM indicates dianhydrides, 4,4'-(Hexafluoroisopropylidene)diphthalic anhydride - diamine diaminomesitylene) MMM revealed a difference in the intra-ZIF-8 transport properties between the embedded ZIF-8 particles and a packed bed of ZIF-8 [18,19]. Although the observed effect was small, it represents the first direct experimental observation of the influence of the ZIF crystal confinement in a polymer on intra-ZIF diffusion. A tentative explanation of this effect has been that the confinement of the

* Corresponding author.

E-mail address: svasenkov@che.ufl.edu (S. Vasenkov).

<https://doi.org/10.1016/j.micromeso.2018.07.044>

Received 28 May 2018; Received in revised form 13 July 2018; Accepted 27 July 2018

Available online 27 July 2018

1387-1811/ © 2018 Elsevier Inc. All rights reserved.

ZIF particles leads to a reduced flexibility of the ZIF framework [18,19]. Comparison of the separation performance and properties of ZIF-90/Matrimid and ZIF-8/Matrimid MMMs at different vol-% of ZIF to the properties of their pure ZIF counterparts led an independent group of authors to the same conclusion [3]. To further understand this confinement phenomenon, detailed diffusion studies of more ZIF based MMMs with varied ZIFs and polymer matrices can be beneficial. Already, ZIF-11 has been discussed as a potentially interesting candidate as a filler material for MMMs in both experimental [13,14] and simulation studies [6], primarily due to its small pore aperture size of 3.0 Å – 3.3 Å and its cage size of 14.6 Å, which support its appropriate structural characteristics for molecular sieving [20,24]. Furthermore, ZIF-11 has comparable chemical and thermal stability with the same metallic center as ZIF-8 [13,20].

Here we report microscopic studies of diffusion of ethylene at different ethylene loadings in ZIF-11 bed and in the following ZIF-11 based MMMs: a ZIF-11/Torlon, ZIF-11/Matrimid, and ZIF-11/6FDA-DAM. Diffusion measurements were performed using ^{13}C PFG NMR utilizing a high field (17.6 T or 14 T) and high magnetic field gradients (up to 25 T/m) to obtain diffusivities for the length scales of displacements smaller than the mean size of the ZIF-11 crystals. These studies provided direct information of the influence of the confinement of ZIF-11 crystals in the studied polymers on the intra-ZIF diffusivity of ethylene molecules.

2. Experimental

2.1. Preparation of ZIF -11

ZIF-11 crystals were prepared through modified solvothermal synthesis protocol reported by He et al. [25]. Fig. 1A shows a representative image of the ZIF-11 sample. The crystal size distributions and the mean crystal sizes are given, respectively, in Fig. S1 and Table S1. About 600 mg (4.91 mmol) benzimidazole (Alfa Aesar) was added to a mixture solution of 16.75 g methanol (VWR International) and 3.75 g 18% ammonium hydroxide solution. About 550 mg (2.46 mmol) of $\text{Zn}(\text{O}_2\text{CCH}_3)_2 \cdot 2\text{H}_2\text{O}$ (Alfa Aesar) was added to a mixture solution of 16.8 g methanol (VWR International) and 13.0 g toluene (VWR

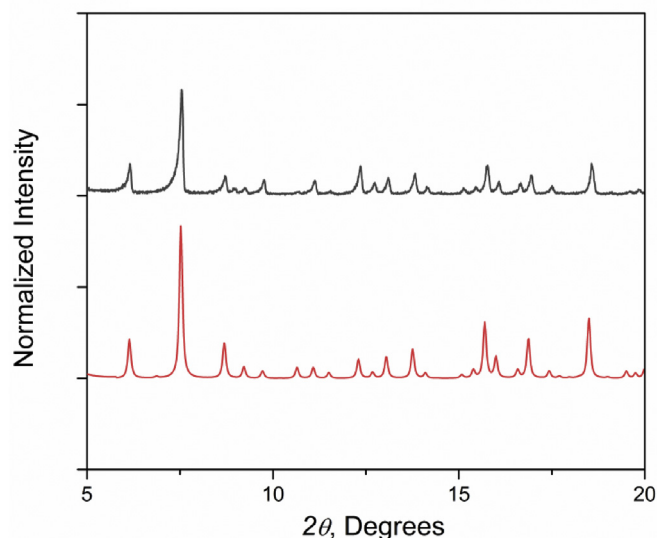


Fig. 2. Powder XRD patterns of the measured ZIF-11 sample (upper pattern) and simulated ZIF-11 (lower pattern) [20].

International). The latter solution was added to the former and stirred for 2 h at room temperature. Note that the reaction time should be precisely controlled to avoid the formation of larger crystals. The ZIF-11 product was recovered by vacuum filtration with methanol washing in the case of powder samples and by centrifugation for use in mixed matrix membranes. The product was activated at 403 K under dynamic vacuum for 24 h. The powder x-ray diffraction patterns reveal a highly crystalline product that is well-matched to the simulated pattern from the literature (Fig. 2).

2.2. 6FDA-DAM synthesis

6FDA-DAM was synthesized following protocols as published in Ref. [26]. A brief and high level description will follow, both 6FDA

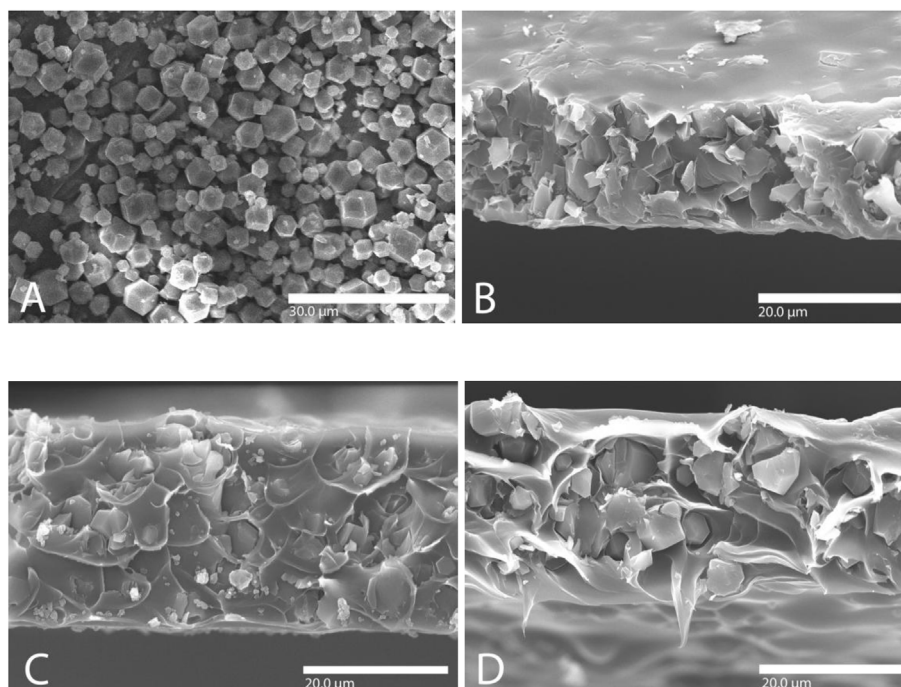


Fig. 1. SEM images of ZIF-11 (A) and ZIF-11 based mixed matrix membranes using the base polymer of Torlon[®] (B), Matrimid[®] (C), and 6FDA-DAM (D).

(dianhydrides, 4,4'-(Hexafluoroisopropylidene)diphthalic anhydride) (BTC) and DAM (diamine diaminomesitylene) (Sigma Aldrich) were dried under vacuum at room temperature before purification. The monomers were further purified in a sublimation apparatus at 488 K (6FDA) and 373 K (DAM) under 100 mTorr vacuum. The sublimated monomers were then stored under dynamic vacuum. Separately, NMP (N-Methyl-2-pyrrolidone) (VWR International) and acetic anhydride (Sigma Aldrich) solvents were dried using activated molecular sieves (3A type). Reactors were purged with N₂ and propane torched under inert purging before the formation of the polyamic acid. The sublimated DAM monomer was dissolved into NMP under stirring and inert purging while being cooled within an ice-water bath. The 6FDA monomer was added into the former solution to polymerize the polyamic acid. Beta-picoline was added to start the chemical imidization after 24 h of polymerization of the polyamic acid. The mass ratio of beta-picoline and acid anhydride utilized was 1:10. Acetic anhydride was added when the beta-picoline was completely dissolved. The final polymer product was precipitated into methanol, followed by extensive washing with fresh methanol. The product was dried under dynamic vacuum at 473 K for 24 h.

2.3. MMM synthesis

Polymers used in this work were either synthesized from monomers (6FDA-DAM) or purchased commercially in the case of Torlon® 4000T-HV (Solvay) and Matrimid® 5218 (Huntsman). The compressive moduli of these polymers have been reported as follows: Torlon (4.5 GPa [27,28]), Matrimid (3.5 GPa [29]), and 6FDA-DAM (1.2 GPa [30]).

The polymer was dried at 383 K under dynamic vacuum for 24 h. 50 mg of polymer powder was dissolved in 10 g N-Methyl-2-pyrrolidone solvent (BDH) in a 20 ml sample vial to form a dilute polymer solution (a so-called “prime dope”). In this solution, 70 mg of ZIF-11 crystals were dispersed with the use of a sonication horn (Branson). After the dispersion step, another 580 mg of dry polymer powder was added to the prime dope and mixed on a rolling mixer over 72 h to fully dissolve the polymer. MMMs of Torlon, Matrimid, and 6FDA-DAM were made separately. Chemical structures of these polymers can be seen in Figs. S2–S4, respectively [31–33].

The membrane dope was degassed overnight before casting to prevent non-selective holes formed via gas bubbles from evaporating solvent. A standard knife casting technique was utilized to fabricate the mixed matrix dense films in a clean glove bag purged with N₂ three times. The as-cast membranes were kept in a solvent-saturated sealed glove bag at 323 K for over 72 h, after which they were annealed at 473 K under dynamic vacuum for 24 h. Selected SEM images of formed MMMs are shown in Fig. 1 B–D.

2.4. PFG NMR sample preparation

The ZIF-11 powder was loosely packed inside a 5 mm (thin walled) NMR tube (Wilmad Labglass, Inc.), reaching a height of about 18 ± 3 mm. The films of polymers and mixed matrix membranes were rolled into cylinders with the diameter of around 4 mm and the length of about 30 ± 3 mm. Each roll was placed into a 5 mm NMR tube. All samples were activated by attaching their respective tube containing the sample to a custom-made vacuum system, gradually increasing the sample temperature under high vacuum to 423 K, and leaving it under high vacuum at this temperature for at least 10 h to remove any sorbates present in the sample. Once the sample had been activated at 423 K, the sample was cooled back to around 296 K under high vacuum and sorbate loading was performed. The sorbate used for this study was ¹³C₂-enriched ethylene (C₂H₄) consisting of a 99% isotopic purity (Sigma-Aldrich). C₂H₄ was loaded into the samples by cryogenically condensing the desired amounts into the NMR tubes using liquid nitrogen. The tubes were flame-sealed upon sorbate loading and separated from the vacuum system. Samples requiring small sorbate

loadings were also loaded by exposing porous material in the NMR tube to the desired ethylene pressure (< 1 bar) at 296 K for at least 2 h, the loading time after which no changes in the amount adsorbed were observed based on the measured NMR signal of ethylene. The sample tubes were flame sealed upon loading.

The sorbate loadings in each material were determined by comparing the NMR signal of ethylene in the studied samples with the NMR signal of bulk ethylene gas at a known pressure in a similar way as discussed in Ref. [34]. For the samples loaded by cryogenic condensation, the following procedure was used. Sealed NMR tubes with porous sample were placed upside down (gas-filled volume is below the porous material) to measure the NMR signal from the gas phase of the NMR tube. A gas-permeable Doty Susceptibility Plug (Wilmad Labglass, Inc.) was placed inside the NMR tubes to prevent the porous material from falling down. NMR signal of the gas region of the samples was compared to that of the reference sample containing only ethylene gas at a known pressure (no porous material added) to obtain sorbate pressure in the gas phase of the samples with porous materials. Sorbate loadings of porous materials were obtained by subtracting the amount of gas in the gas phase of a sample tube from the known total amount of gas in the sample tube. Table 1 shows ethylene loading pressure and concentration in ZIF-11 bed and MMM samples studied in this work.

2.5. NMR measurements

PFG NMR diffusion measurements were performed using a 17.6 T Avance III HD spectrometer (Bruker Biospin) and 14 T Avance III spectrometer (Bruker Biospin) operating at the ¹³C resonance frequencies of 188.6 MHz and 149.8 MHz, respectively. ¹³C PFG NMR was used instead of more traditional ¹H PFG NMR to take advantage of much longer T₂ NMR relaxation times for ¹³C than those expected for protons of guest molecules in ZIFs. In particular, in our recent work we have reported ¹³C T₂ NMR relaxation times of gases in ZIF-11 that were more than a factor of 3 longer than those for protons for the same molecules [35]. As a result, in comparison to ¹H PFG NMR data, the results obtained by ¹³C PFG NMR in ZIFs can be expected to be more representative because a larger fraction of the maximum spin echo signal is recorded. Furthermore, disturbing magnetic susceptibility effects, which might not be completely removed by the bipolar 13-interval PFG NMR sequence, are much less for ¹³C than for ¹H. Sine-shaped and trapezoidal-shaped, bipolar magnetic field gradients with the effective duration of 2–2.5 ms and amplitudes up to 25 T/m and 18 T/m were generated using Diff50 and Diff30 diffusion probes (Bruker BioSpin), respectively. The effective diffusion time varied between 30 and 270 ms, and the time between the first and second π/2

Table 1
Loading pressure and concentration of ethylene in the ZIF-11 and MMM samples obtained using NMR signal analysis.

Sample	Loading pressure ^a at 296 K, bar	Sorbate loading ^b at 296 K, mmol/g
ZIF-11 packed bed	0.8	1.2
ZIF-11 packed bed	2.0	1.7
ZIF-11 packed bed	9.0	3.1
ZIF-11/Torlon MMM	0.8	0.06
ZIF-11/Torlon MMM	2.2	0.40
ZIF-11/Torlon MMM	9.1	1.5
ZIF-11/Matrimid MMM	0.8	0.07
ZIF-11/Matrimid MMM	9.1	1.1
ZIF-11/6FDA-DAM	0.8	0.34
MMM		
ZIF-11/6FDA-DAM	2.4	0.85
MMM		
6FDA-DAM Polymer	0.8	0.17

^a 15% experimental uncertainty.

^b 25% experimental uncertainty.

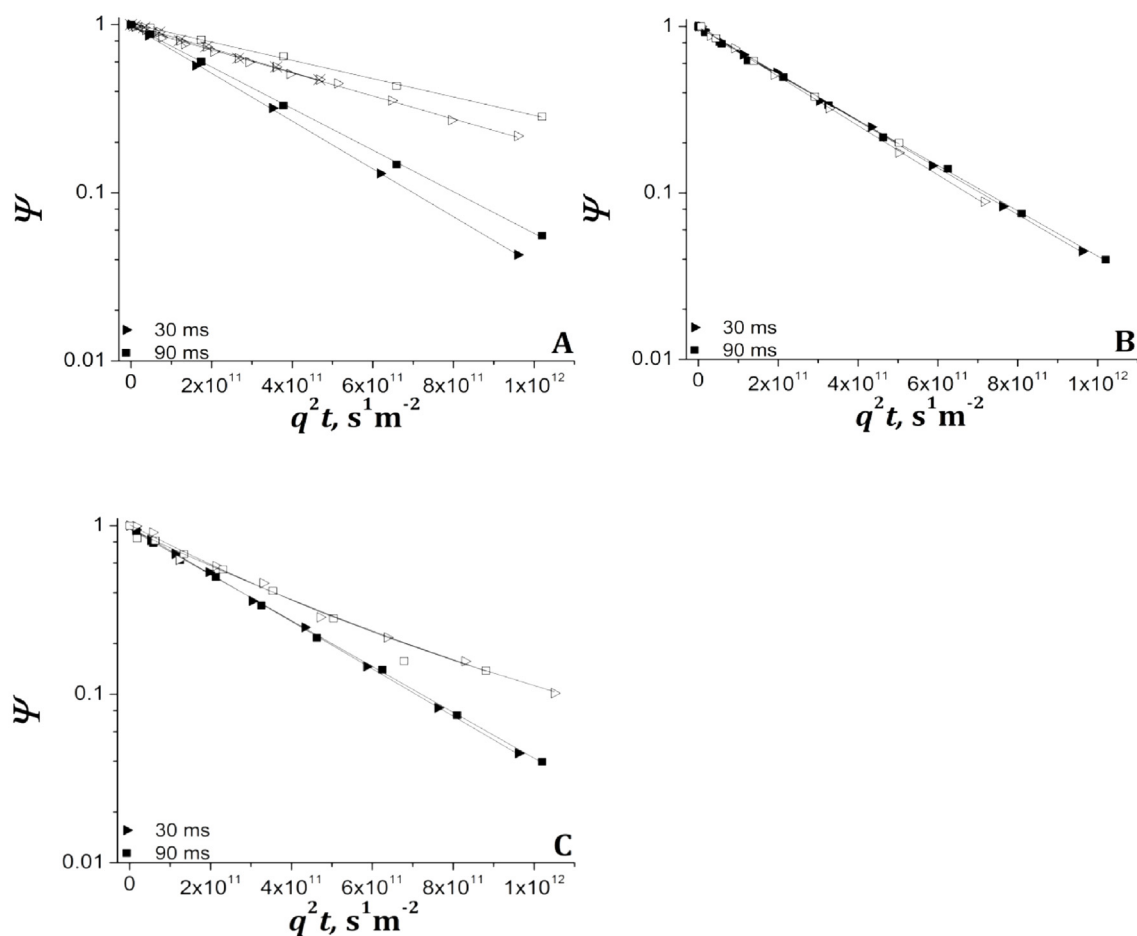


Fig. 3. ^{13}C PFG NMR attenuation curves measured for intra-ZIF diffusion of ethylene at low loadings corresponding to the loading pressure of 0.8 bar at 296 K for a bed of ZIF-11 crystals (filled symbols) and in ZIF-11 based MMMs (hollow symbols). MMMs were prepared using the polymers Torlon (A), Matrimid (B), and 6FDA-DAM (C). The measurements were performed for different diffusion times at 296 K and 17.6 T. Also shown for comparison in Figure A are the corresponding attenuation data obtained at 14 T for Torlon MMM (symbols with crosses). The solid lines represent the results of least-square fitting using Eq. (1) for Torlon and Matrimid and Eq. (3) for 6FDA-DAM.

radiofrequency pulses of the 13-interval sequence was 8.5 ms. The reported NMR data were obtained after keeping the samples at 296 K inside the magnet for at least 1 h to ensure the sorption equilibrium conditions in the sample. This 1 h equilibration was performed in addition to at least 2 h equilibration at essentially the same temperature outside the magnet. It was verified that the measured NMR data do not depend on the time in the magnet after the initial equilibration. In particular, the NMR signal, which is proportional to the total number of sorbate molecules in the ZIF-11 crystal bed or MMM, was monitored during the measurements that lasted several days at 296 K. There were no changes in the signal indicating no change in the gas concentration inside the bed. Hence, all reported NMR data correspond to the condition of sorption equilibrium at 296 K. Diffusion measurements were performed using the 13-interval PFG NMR pulse sequence with bipolar gradients [36], modified by the addition of a longitudinal eddy current delay. The diffusivities were obtained from the measured PFG NMR attenuation curves, i.e., dependencies of the PFG NMR signal intensity on the effective magnetic field gradient strength (g) with all other pulse sequence parameters held fixed. PFG NMR signal intensities were obtained for ethylene by integration of the corresponding NMR spectra. Under our measurement conditions, the ^{13}C NMR spectrum of C_2H_4 consisted of a single line at around 120.5 ppm. In the case of normal self-diffusion with a single diffusion coefficient (D), PFG NMR attenuation curves can be presented as [37–40].

$$\psi = \frac{S(g)}{S(g \approx 0)} = \exp(-Dq^2t) \quad (1)$$

where ψ is the PFG NMR signal attenuation, S is the PFG NMR signal intensity, t is the time of observation of the diffusion process (i.e., diffusion time) and $q = 2\gamma g\delta$, where γ is the gyromagnetic ratio and δ is the effective gradient pulse length. In the case of normal self-diffusion in three dimensions, the mean square displacement (MSD) is related to D and t by the Einstein relation

$$\langle r^2 \rangle = 6Dt. \quad (2)$$

For a diffusion process involving two molecular ensembles diffusing with different diffusivities, Eq. (1) can be re-written as [37,38].

$$\psi = \frac{S(g)}{S(g \approx 0)} = \sum_i^{n=2} p_i \exp(-D_i q^2 t) \quad (3)$$

where, p_i and D_i are, respectively, the phase fraction and self-diffusivity of ensemble i .

The uncertainty of the diffusivities reported in the paper is based on the reproducibility of the diffusion data measured with 2–3 identically prepared (but different) NMR samples. Hence, the uncertainty of the loading contributes to the uncertainty of the reported diffusivities. The uncertainty of the diffusivities is also based on the reproducibility of the data measured with the same samples but at different fields (17.6 and 14 T) and using different diffusion probes (Diff50 and Diff30).

Longitudinal (T_1) and transverse (T_2) NMR relaxation times were

estimated using the 13-interval PFG NMR sequence. For T_1 relaxation times, the measurements were performed by changing the time interval between the second and third $\pi/2$ radiofrequency pulses of the sequence while keeping all other time intervals constant. For T_2 relaxation times, the measurements were performed by changing the time interval between the first and second $\pi/2$ radiofrequency pulses of the sequence. Under the conditions of these measurements, it was ensured that there was no attenuation of the signal due to sorbate diffusion inside ZIF-11 crystals or MMM. At the same time, all signal from the gas phase of the sample was completely suppressed by the applied gradients. As a result, the reported T_1 and T_2 relaxation times correspond to ethylene located inside microporous samples. The relaxation measurements were performed using the 13-interval PFG NMR sequence because such measurements provide a direct approach to estimate the total loss of the signal in the diffusion measurements using this sequence due to NMR relaxation. As a high magnetic field and complex samples are used, measured NMR relaxation times are susceptible to depend on the NMR sequence used. T_1 relaxation was found to range from 0.3 to 2 s, and T_2 relaxation was found to range from 4.2 to 9 ms (Table S2). All NMR relaxation data were consistent with the absence of any distribution over T_1 and T_2 relaxation times. All NMR studies reported in this work were performed at 296 K.

3. Results and discussion

Figs. 3 and 4 show the ^{13}C PFG NMR attenuation curves measured at 17.6 T for ethylene diffusion in ZIF-11/polymer MMMs and the

corresponding ZIF-11 beds for the low and high ethylene loadings used in this work, respectively. It is important to note that in all cases the measured bed of ZIF-11 crystals was from the same batch of crystals used to synthesize the corresponding MMM. In each of the A, B, and C figures, the attenuation data for a particular ZIF-11 based MMM are compared with the data for the corresponding ZIF-11 bed at the same, within uncertainty, ethylene loading pressure, which ensures the same intra-ZIF ethylene loading in the MMM and bed. The high ethylene loading data in Fig. 4 correspond to the loading pressure of 9.1 bar for ZIF-11/Torlon and ZIF-11/Matrimid MMM. However, a loading pressure of only 2.4 bar was used for ZIF-11/6FDA-DAM MMM as the 6FDA-DAM polymer shows plasticization effects at 9.1 bar. Fig. S6 presents the comparison of the attenuation data for Torlon MMM and ZIF-11 bed at an additional ethylene loading pressure. To confirm the absence of magnetic susceptibility effects and/or other measurement artifacts under our experimental conditions, complementary diffusion measurements were performed using ^{13}C PFG NMR at a lower field of 14 T. The attenuation curves in Figs. 3, 4, and S6 measured at 14 T are seen to coincide, within uncertainty, with the respective ^{13}C PFG NMR attenuation curves measured for the same samples and under the same conditions at 17.6 T. Such agreement confirms the absence of any magnetic susceptibility effects and/or any measurement artifacts under our experimental conditions.

It can be seen that the ^{13}C attenuation curves corresponding to the ZIF-11/Torlon (Figs. 3A, 4A, S6) and ZIF-11/Matrimid (Figs. 3B and 4B) MMMs exhibit monoexponential behavior (i.e., linear in the semi-logarithmic presentation of the figure) with respect to q^2 in agreement

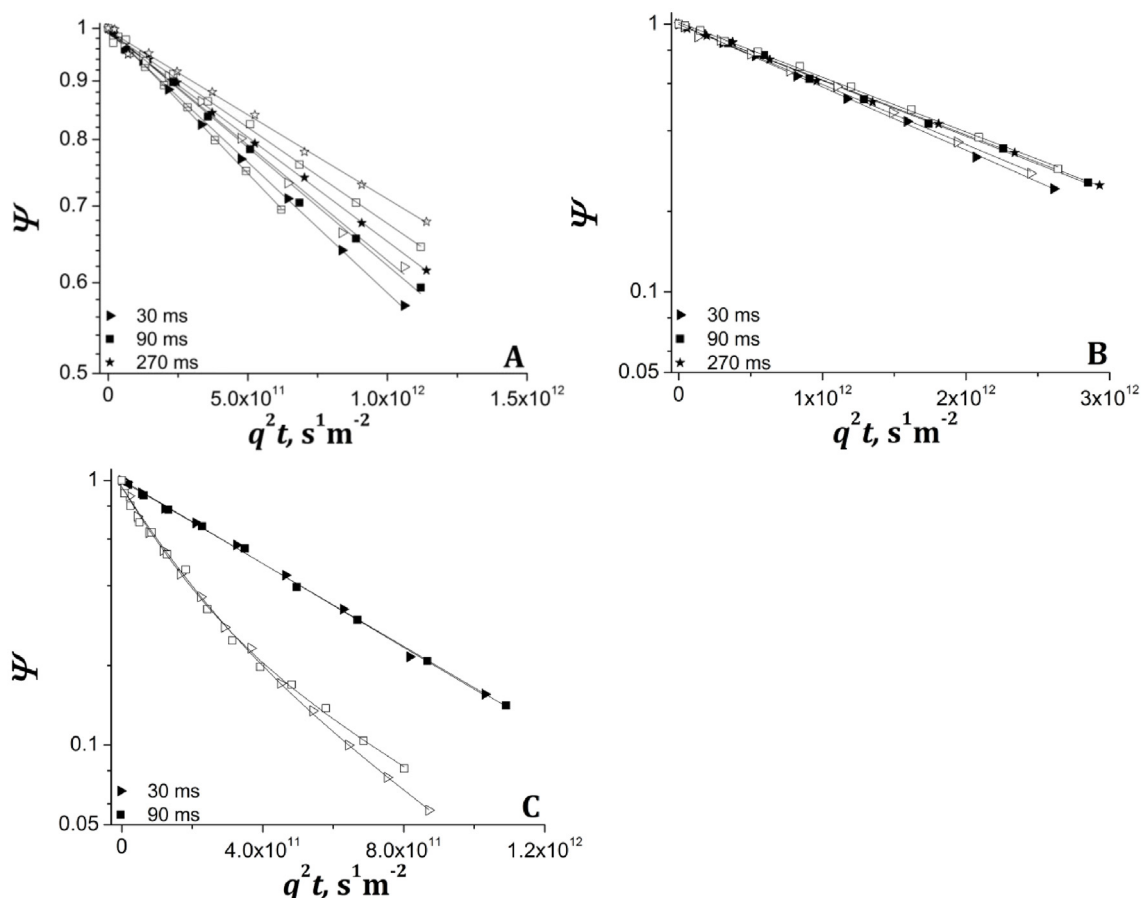


Fig. 4. ^{13}C PFG NMR attenuation curves measured for intra-ZIF diffusion of ethylene at high loadings for a bed of ZIF-11 crystals (filled symbols) and in ZIF-11 based MMMs (hollow symbols). MMMs were prepared using the polymers Torlon (A), Matrimid (B), and 6FDA-DAM (C). The ethylene loading pressures to prepare the MMM and bed samples were 9.1 bar (A), 9.1 bar (B), and 2.4 bar (C). The measurements were performed for different diffusion times at 296 K and 17.6 T. Also shown for comparison in Figure A are the corresponding attenuation data obtained at 14 T for a bed of ZIF-11 crystals (open squares with a dash). The solid lines represent the results of least-square fitting using Eq. (1) for Torlon and Matrimid and Eq. (3) for 6FDA-DAM.

with Eq. (1). This observation indicates that, for any particular diffusion time, there is a single diffusivity for these studied samples. These diffusivities are assigned to diffusion inside the crystals of ZIF-11 confined in the MMMs. This assignment is based on the observation that the intra-polymer diffusion does not contribute to the measured attenuation curves because of the low T_2 relaxation times combined with low gas loadings in the polymer phases. The latter was confirmed by the NMR measurements of the pure polymer films loaded with ethylene. Furthermore, any signal originated from molecules that diffuse in the gas phase of the sample for at least a fraction of diffusion time was attenuated away already at the smallest gradient strength used in the measurements. For the case of the ZIF-11/6FDA-DAM MMM, it can be seen that the ^{13}C attenuation curves deviate from monoexponential behavior (Figs. 3C and 4C). Here, the intra-polymer diffusion contributes to the measured attenuation curves as observed in our previous studies for a MMM made of the same type of the polymer and a different ZIF [18,19]. In this case, the intra-polymer diffusion is observable by ^{13}C PFG NMR because T_2 ^{13}C NMR relaxation time of ethylene in 6FDA-DAM as pure polymer is sufficiently large (Table S2). Hence, for ZIF-11/6FDA-DAM MMM, observation of two molecular ensembles (one diffusing inside ZIF-11 crystals and another in the polymer phase surrounding the crystals) is expected by ^{13}C PFG NMR at sufficiently small times when the molecular exchange between the crystals and the polymer can be neglected. As a result, Eq. (3), which considers the existence of two diffusing ensembles, was used to fit the attenuation curves for this MMM. At the same time, Eq. (1) is valid for a single diffusivity and was applied for the remaining two MMMs and for ZIF-11 beds. The results of least squares fitting of the attenuation curves using these equations are shown in Tables 2–4, respectively, for ZIF-11/Torlon, ZIF-11/Matrimid and ZIF-11/6FDA-DAM MMMs as well as the respective ZIF-11 bed samples. The corresponding least square fitting data for ZIF-11/Torlon at the additional ethylene loading pressure of 2.2 bar (Fig. S6) are presented in Table S3. Tables 2–4 and S3 also show the corresponding root MSD values obtained using Eq. (2).

To ensure the correct assignment of the two diffusion ensembles observed for ZIF-11/6FDA-DAM MMM to intra-ZIF and intra-polymer diffusion, the diffusivities in Table 4 were compared with the previously measured ethylene diffusivity at a high loading pressure [19] and with the corresponding diffusivity measured in this work at a low loading pressure (Fig. S7) in a film of pure 6FDA-DAM polymer. The attenuation curves of the 6FDA-DAM polymer (Fig. S7) show no dependence on diffusion time, coinciding onto a single line. The least square fitting of these data by Eq. (1) revealed the intra-polymer diffusivity to be equal to $(2.0 \pm 0.2) \times 10^{-12} \text{ m}^2/\text{s}$. Comparison of this diffusivity to that in Table 4 shows that the intra-polymer diffusivity slightly decreased through the formation of the MMM. We have previously reported such intra-polymer diffusivity decrease for the case of ZIF-8/6FDA-DAM MMM, which can be attributed to the polymer chain rigidification induced by the MMM formation [18,19]. It should be noted that for the ZIF-11/6FDA-DAM MMM sample, using Eq. (3) to fit the data results in a larger total experimental error of the intra-ZIF diffusivities compared to fitting all the other data with Eq. (1). This is due to the nature of biexponential fits (Eq. (3)); in which four fitting parameters are used

instead of a single fitting parameter in monoexponential fits (Eq. (1)). Furthermore, it can be seen in Table 4, that at higher loadings in ZIF-11/6FDA-DAM MMM sample, the majority of the measured PFG NMR signal is from the polymer phase, which makes the uncertainty of the diffusivity in the ZIF-11 phase even larger.

The diffusion data in Tables 3 and 4 and Figs. 3 and 4 show that for ZIF-11/Matrimid, ZIF-11/6FDA-DAM MMMs, and their respective beds of ZIF-11 crystal batches no dependence of diffusivities on the diffusion time is observed, within uncertainty. However, for ZIF-11/Torlon MMM and its respective batch of ZIF-11 (Tables 2 and S3 and Figs. 3, 4, S6), the measured diffusion data indicate some weak decrease of intra-ZIF ethylene diffusivity as the diffusion time increases. For ZIF-11 beds, similar time dependence of the diffusivity measured by PFG NMR was previously reported when methane and carbon dioxide were used as sorbates [35]. This dependence was analyzed with formulations presented by Mitra et al. [41–44] and attributed to reflections of diffusing molecules from the external crystal surface that acts as a transport barrier at small diffusion times. Comparison of the root MSD values for ZIF-11/Torlon MMM and the corresponding ZIF-11 bed (Tables 2 and S3) with the average crystal size of $3.1 \mu\text{m}$ (Table S1) indicate that these values are similar and, as a result, the observed dependence of the diffusivities on diffusion time can be assigned to the effects at the external crystal surface. The observed time dependence was not sufficiently strong for detailed, quantitative studies of these effects. For the other two MMMs and the corresponding ZIF-11 beds, such effects were less pronounced or absent because of the larger average ZIF-11 crystal sizes in these samples (Table S1).

The results in Tables 2 and S3 show that the intra-ZIF diffusivities of ethylene in the ZIF-11/Torlon MMM are consistently smaller than the corresponding diffusivities measured under the same conditions in the ZIF-11 bed, with the largest difference of around a factor of 2 observed for the low and intermediate ethylene loadings. At the same time, the results in Tables 3 and 4 indicate that the intra-ZIF diffusivities of ethylene in ZIF-11/Matrimid and ZIF-11/6FDA-DAM MMMs are the same, within uncertainty, as those in the corresponding ZIF-11 beds under the same measurement conditions. Ratios of intra-ZIF diffusivities of ethylene in the ZIF-11 beds and ZIF-11 based MMMs for different comparable ethylene loading pressures are shown in Table 5. For the samples that showed a time-dependence in the diffusivity (i.e., ZIF-11/Torlon MMM), the ratios were calculated using the diffusivities measured at the smallest diffusion times when any effects at the external crystal surface on the measured diffusivity can be considered to be negligibly small or nonexistent. Alternatively, for samples that showed, within uncertainty, no time-dependence (i.e., ZIF-11/Matrimid MMM and ZIF-11 6FDA-DAM MMM), the ratios were calculated based on the average diffusivity over all diffusion times used. Smaller intra-ZIF diffusivity in a MMM in comparison with that in the corresponding ZIF bed was previously observed by PFG NMR for ZIF-8/6FDA-DAM MMM [18,19]. The diffusivity reduction effect for ZIF-8/6FDA-DAM MMM was much smaller than the factor of 2 decrease observed in this work for ZIF-11/Torlon MMM. Despite this quantitative difference we believe that the origin of the diffusivity reduction is the same for both MMMs, i.e. the reduced flexibility of the framework of ZIF crystals due

Table 2

PFG NMR data for intra-ZIF diffusion obtained at 296 K in ZIF-11/Torlon MMM compared to ZIF-11 bed with the same ethylene loading pressure. Also shown are the root MSD calculated using Eq. (2).

Loading Pressure ^a (ZIF-11), bar	Loading Pressure ^a (MMM), bar	Diffusion Time, ms	$D(\text{bed}), 10^{-12} \frac{\text{m}^2}{\text{s}}$	Root MSD (bed), μm	$D(\text{MMM}), 10^{-12} \frac{\text{m}^2}{\text{s}}$	Root MSD (MMM), μm
0.8	0.8	30	3.3 ± 0.3	0.74 ± 0.04	1.6 ± 0.2	0.51 ± 0.05
0.8	0.8	90	2.8 ± 0.3	1.2 ± 0.1	1.3 ± 0.1	0.81 ± 0.05
9.0	9.1	30	0.53 ± 0.05	0.29 ± 0.01	0.46 ± 0.05	0.28 ± 0.01
9.0	9.1	90	0.47 ± 0.05	0.50 ± 0.03	0.39 ± 0.04	0.45 ± 0.03
9.0	9.1	270	0.42 ± 0.05	0.82 ± 0.05	0.34 ± 0.04	0.74 ± 0.05

^a 15% experimental uncertainty.

Table 3

PFM NMR data for intra-ZIF diffusion obtained at 296 K in ZIF-11/Matrimid MMM compared to ZIF-11 bed with the same ethylene loading pressure. Also shown are the root MSD calculated using Eq. (2).

Loading Pressure ^a (ZIF-11), bar	Loading Pressure ^a (MMM), bar	Diffusion Time, ms	$D(\text{bed}), 10^{-12} \frac{\text{m}^2}{\text{s}}$	Root MSD (bed), μm	$D(\text{MMM}), 10^{-12} \frac{\text{m}^2}{\text{s}}$	Root MSD (MMM), μm
0.8	0.8	30	3.2 ± 0.3	0.7 ± 0.06	3.4 ± 0.3	0.75 ± 0.07
0.8	0.8	90	3.1 ± 0.3	1.3 ± 0.1	3.2 ± 0.3	1.3 ± 0.1
9.0	9.1	30	0.54 ± 0.05	0.30 ± 0.01	0.52 ± 0.05	0.29 ± 0.01
9.0	9.1	90	0.48 ± 0.05	0.50 ± 0.03	0.47 ± 0.05	0.50 ± 0.05
9.0	9.1	270	0.47 ± 0.05	0.87 ± 0.05	–	–

^a 15% experimental uncertainty.

to the confinement in the polymer [18,19]. The higher bulk modulus of Torlon (4.5 GPa) in comparison with those of 6FDA-DAM (1.2 GPa) and Matrimid (3.5 GPa) used in this work can be the main reason for stronger confinement effects observed in ZIF-11/Torlon MMM than in the other two studied MMM. Finally, the observed absence of reduced intra-ZIF diffusivity in this work for ZIF-11/6FDA-DAM MMM compared to the previous observation of such reduction for ZIF-8/6FDA-DAM MMM needs to be further explored. The lack of the diffusivity reduction in the former MMM might be related to properties of ZIF/polymer interface, which can be expected to be somewhat different for different ZIFs.

The intra-ZIF diffusivities measured for each sample at the smallest diffusion time when the effects at the external crystal surface are small or nonexistent are compared as a function of ethylene loading pressure in Fig. 5. It is seen in the figure that for both ZIF-11 and ZIF-11 based MMMs, an increase in ethylene loading pressure causes a reduction in the intra-ZIF diffusivity of ethylene molecules, a trend previously observed in other microporous materials [37,45]. Such a trend can be explained by the mutual hindrance experienced by diffusing molecules. Such hindrance is increased with molecular concentration. In our opinion, it is possible that at high sorbate loadings ZIF-11 framework flexibility is partially restricted by adsorbed molecules. In particular, linker reorientation might be restricted if guest molecules are hindering such reorientation movements due to guest-linker interaction or a reduction in the available free volume by guest molecules. However, it is difficult to deconvolute this effect on diffusion from the mutual hindrance phenomena previously mentioned. Such flexibility restriction can be of similar manner to that caused by a confinement when embedded in Torlon. It is also possible that ethylene gas adsorbed in Torlon at the high pressure used in this study causes some plasticization effects in the polymer that reduce the extent of confinement of ZIF-11 crystals in ZIF-11/Torlon MMM. Both of these effects can explain a much lower extent of the intra-ZIF diffusivity reduction due to confinement of ZIF-11 crystals in Torlon at the highest ethylene loading pressure (Fig. 5 and Table 5).

4. Conclusion

¹³C PFG NMR at 17.6 T was used to compare the intra-ZIF diffusivities inside ZIF-11 based MMMs to the corresponding diffusivities in

Table 4

PFM NMR diffusion data obtained at 296 K in ZIF-11/6FDA-DAM MMM compared to ZIF-11 bed with the same or similar ethylene loading pressure. Also shown are the root MSD calculated using Eq. (2).

Loading Pressure ^a (ZIF-11), bar	Loading Pressure ^a (MMM), bar	Diffusion Time, ms	$D(\text{bed}), 10^{-12} \frac{\text{m}^2}{\text{s}}$	Root MSD (bed), μm	$D_1, 10^{-12} \frac{\text{m}^2}{\text{s}}$ Polymer ensemble	$D_2, 10^{-12} \frac{\text{m}^2}{\text{s}}$ ZIF-11 ensemble	p_1	p_2	Root MSD (MMM) 1, μm	Root MSD (MMM) 2, μm
0.8	0.8	30	3.2 ± 0.3	0.7 ± 0.06	1.3 ± 0.4	3.6 ± 0.4	0.33	0.67	0.46 ± 0.05	0.77 ± 0.04
0.8	0.8	90	3.1 ± 0.3	1.3 ± 0.1	1.5 ± 0.3	3.4 ± 0.3	0.41	0.59	0.87 ± 0.1	1.3 ± 0.1
2.0	2.4	30	1.8 ± 0.2	0.55 ± 0.03	6.5 ± 0.6	2.2 ± 0.3	0.59	0.41	1.0 ± 0.1	0.61 ± 0.04
2.0	2.4	90	1.8 ± 0.2	0.97 ± 0.06	6.9 ± 0.7	1.8 ± 0.3	0.63	0.37	1.9 ± 0.1	0.98 ± 0.1

^a 15% experimental uncertainty.

Table 5

Ratios of intra-ZIF diffusivities of ethylene in the ZIF-11 beds and ZIF-11 based MMMs at different ethylene loading pressures.

MMM Type	Loading Pressure ^a , Bar	Ratio ^b ($D_{\text{bed}}/D_{\text{MMM}}$)
ZIF-11/Torlon MMM	0.8	2.1
ZIF-11/Torlon MMM	2.2	1.8
ZIF-11/Torlon MMM	9.1	1.2
ZIF-11/Matrimid MMM	0.8	1.0
ZIF-11/Matrimid MMM	9.1	1.0
ZIF-11/6FDA-DAM MMM	0.8	0.90
ZIF-11/6FDA-DAM MMM	2.4	0.90

^a 15% experimental uncertainty.

^b 20% experimental uncertainty.

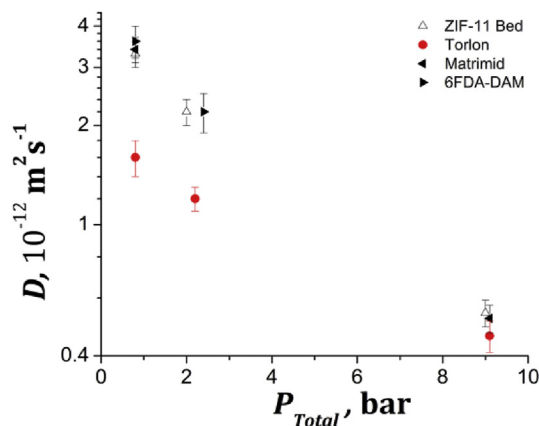


Fig. 5. Diffusivity as a function of loading pressure of ethylene in ZIF-11 and ZIF-11 based MMMs. Diffusivities were based off the shortest diffusion time used in the measurements.

ZIF-11 crystal beds. Selected diffusion measurements were also performed using ¹³C PFG NMR at 14 T. The observation of the diffusion results at two different field strengths (17.6 T and 14 T) that were the same, within uncertainty, rules out any potential measurement artifacts in the reported studies. It was observed that the intra-ZIF diffusivity of

ethylene in ZIF-11 beds was about twice that of the intra-ZIF diffusivity inside the ZIF-11/Torlon MMM at low and intermediate ethylene loadings. Such an effect has been reported before, although not nearly as large, for ZIF-8/6FDA-DAM and can be explained by the flexibility of the ZIF-11 framework being restricted by the crystal confinement in MMMs. At the same time, no intra-ZIF diffusivity reduction was observed for the other two studied MMMs, ZIF-11/Matrimid and ZIF-11/6FDA-DAM. This observation was tentatively attributed to the higher bulk modulus of Torlon than those of Matrimid and 6FDA-DAM. It was observed that an increase of the ethylene loading inside ZIF-11 crystals leads to a decrease in the intra-ZIF diffusivity as well as in a reduction in the effect of ZIF-11 confinement inside ZIF-11/Torlon MMM on the intra-ZIF diffusivity.

Acknowledgements

We are grateful for the financial support of this work by NSF (CBET awards No. 1510411 and No. 1510442). A portion of this work was performed in the McKnight Brain Institute at the National High Magnetic Field Laboratory's AMRIS Facility, which is supported by National Science Foundation Cooperative Agreement No. DMR-1157490 and the State of Florida. This work was supported in part by an NIH award, S10RR031637, for magnetic resonance instrumentation. The authors thank Dr. Brian Pimentel for his helpful comments and suggestions on the manuscript.

Appendix A. Supplementary data

Supplementary data related to this article can be found at <https://doi.org/10.1016/j.micromeso.2018.07.044>.

References

- [1] R.W. Baker, *Ind. Eng. Chem. Res.* 41 (2002) 1393–1411.
- [2] M. Freemantle, *Chem. Eng. News* 83 (2005) 49–57.
- [3] L. Diestel, N. Wang, B. Schwiedland, F. Steinbach, U. Giese, J. Caro, *J. Membr. Sci.* 492 (2015) 181–186.
- [4] T. Rodenas, M.v. Dalen, E. García-Pérez, P. Serra-Crespo, B. Zornoza, F. Kapteijn, J. Gascon, *Adv. Funct. Mater.* 24 (2014) 249–256.
- [5] M.J.C. Ordoñez, K.J.B. Jr., J.P. Ferraris, I.H. Musselman, *J. Membr. Sci.* 361 (2010) 28–37.
- [6] G. Yilmaz, S. Keskin, *Ind. Eng. Chem. Res.* 51 (2012) 14218–14228.
- [7] R. Mahajan, W.J. Koros, *Polym. Eng. Sci.* 42 (2002) 1420–1431.
- [8] B.R. Pimentel, A. Parulkar, E.-k. Zhou, N.A. Brunelli, R.P. Lively, *ChemSusChem* 7 (2014) 3202–3240.
- [9] C. Zhang, Y. Dai, J.R. Johnson, O. Karvan, W.J. Koros, *J. Membr. Sci.* 389 (2012) 34–42.
- [10] B. Zornoza, B. Seoane, J.M. Zamaro, C. Téllez, J. Coronas, *ChemPhysChem* 12 (2011) 2781–2785.
- [11] T.-H. Bae, J.S. Lee, W. Qiu, W.J. Koros, C.W. Jones, S. Nair, *Angew. Chem. Int. Ed.* 49 (2010) 9863–9866.
- [12] J. Yao, H. Wang, *Chem. Soc. Rev.* 43 (2014) 4470–4493.
- [13] J. Sánchez-Lainez, B. Zornoza, Á. Mayoral, Á. Berenguer-Murcia, Diego Cazorla-Amorós, C. Téllez, J. Coronas, *J. Mater. Chem.* 3 (2015) 6549–6556.
- [14] M.S. Boroglu, A.B. Yumru, *Separ. Purif. Technol.* 173 (2017) 269–279.
- [15] R.T. Adams, J.S. Lee, Y.-H. Bae, J.K. Ward, J.R. Johnson, C.W. Jones, S. Nair, W.J. Koros, *J. Membr. Sci.* 367 (2011) 197–203.
- [16] S. Keskin, D.S. Sholl, *Energy Environ. Sci.* 3 (2009) 343–351.
- [17] K. Díaz, M. López-González, L.F.d. Castillo, E. Riande, *J. Membr. Sci.* 383 (2011) 206–213.
- [18] R. Mueller, V. Hariharan, C. Zhang, R. Lively, S. Vasenkov, *J. Membr. Sci.* 499 (2016) 12–19.
- [19] R. Mueller, S. Zhang, C. Zhang, R.P. Lively, S. Vasenkov, *J. Membr. Sci.* 477 (2015) 123–130.
- [20] K.S. Park, Z. Ni, A.P. Côté, J.Y. Choi, R. Huang, F.J. Uribe-Romo, H.K. Chae, M. O'Keeffe, O.M. Yaghi, *Proc. Natl. Acad. Sci. U.S.A.* 103 (2006) 10186–10191.
- [21] B.C.Z. Yang, Y. Zhu, Y. Xia, *J. Mater. Chem.* 2 (2014) 16811–16831.
- [22] L. Hertäg, H. Bux, J. Caro, C. Chmelik, T. Remsungnen, M. Knauth, S. Frizsche, *J. Membr. Sci.* 377 (2011) 36–41.
- [23] E. Haldoupis, T. Watanabe, S. Nair, D.S. Sholl, *ChemPhysChem* 13 (2012) 3449–3452.
- [24] E.L. First, C.A. Floudas, *Microporous Mesoporous Mater.* 165 (2013) 32–39.
- [25] M. He, J. Yao, Q. Liu, Z. Zhong, H. Wang, *Dalton Trans.* 42 (2013) 16608–16613.
- [26] R.H. Vora, *Process of Making a Shaped Article from Intermediate Molecular Weight Polyimides*, CNA Holdings Inc, 1990.
- [27] T.L. Mueller, S.E. Basler, R. Müller, G.H.v. Lenthe, *Med. Eng. Phys.* 35 (2013) 636–643.
- [28] S.E. Basler, J. Traxler, R. Müller, G.H.v. Lenthe, *Med. Eng. Phys.* 35 (2013) 1442–1449.
- [29] V.V. Kozey, S. Kumar, *J. Mater. Res.* 9 (2011) 2717–2726.
- [30] D. Harding, F.Y. Tsai, R.Q. Gram, *LLE Review* 92 (2002) 167–180.
- [31] G.P. Robertson, M.D. Guiver, M. Yoshikawa, S. Brownstein, *Polymer* 45 (2004) 1111–1117.
- [32] F. Zhou, W.J. Koros, *Polymer* 47 (2006) 280–288.
- [33] L. Xu, C. Zhang, M. Rungta, W. Qiu, J. Liu, W.J. Koros, *J. Membr. Sci.* 459 (2014) 223–232.
- [34] M. Dvoyashkin, J. Zang, G.I. Yucelen, A. Katihar, S. Nair, D.S. Sholl, C.R. Bowers, S. Vasenkov, *J. Phys. Chem. C* 116 (2012) 21350–21355.
- [35] E.M. Forman, B.R. Pimentel, K.J. Ziegler, R.P. Lively, S. Vasenkov, *Microporous Mesoporous Mater.* 248 (2017) 158–163.
- [36] R.M. Cotts, M.J.R. Hoch, T. Sun, J.T. Markert, *J. Magn. Reson.* 83 (1989) 252–266.
- [37] J. Kärger, D.M. Ruthven, D.N. Theodorou, *Diffusion in Nanoporous Materials*, Wiley-VCH Verlag GmbH & Co. KGaA, Weinheim, Germany, 2012.
- [38] J. Kärger, H. Pfeifer, W. Heink, *Adv. Magn. Reson.* 12 (1988) 1–89.
- [39] E.O. Stejskal, J.E. Tanner, *J. Chem. Phys.* 42 (1965) 288–292.
- [40] P.T. Callaghan, D. MacGowan, K.J. Packer, F.O. Zelaya, *Magn. Reson. Imaging* 9 (1991) 663–671.
- [41] O. Geier, R.Q. Snurr, F. Stallmach, J. Kärger, *J. Chem. Phys.* 120 (2004) 367.
- [42] P.P. Mitra, P.N. Sen, L.M. Schwartz, *Phys. Rev. B Condens. Matter* 47 (1993) 8565–8574.
- [43] P.P. Mitra, P.N. Sen, *Phys. Rev. B Condens. Matter* 45 (1992) 143–156.
- [44] M. Krutyeva, X. Yang, S. Vasenkov, J. Kärger, *J. Magn. Reson.* 185 (2007) 300–307.
- [45] C. Chmelik, J. van Baten, R. Krishna, *J. Membr. Sci.* 397–398 (2012) 87–91.